NATURAL CONVECTION OF AIR IN A SQUARE CAVITY
A BENCH MARK NUMERICAL SOLUTION

G. DE VAHL DAVIS

University of New South Wales, Kensington 2033, Australia

SUMMARY

Details are given of the computational method used to obtain an accurate solution of the equations describing two-dimensional natural convection in a square cavity with differentially heated side walls. Second-order, central difference approximations were used. Mesh refinement and extrapolation led to solutions for $10^3 \leqslant Ra \leqslant 10^6$ which are believed to be accurate to better than 1 per cent at the highest Rayleigh number and down to one-tenth of that at the lowest value.

KEY WORDS   Natural Convection   Numerical Methods   Bench Mark Solution   Square Cavity

INTRODUCTION

Buoyancy-driven flow in a square cavity with vertical sides which are differentially heated is a suitable vehicle for testing and validating computer codes used for a wide variety of practical problems such as nuclear reactor insulation, ventilation of rooms, solar energy collection and crystal growth in liquids.

Following a suggestion to this effect by Jones,[1] contributions were invited[2–4] to the solution of this problem. At the Venice conference on Numerical Methods in Thermal Problems, the contributions were reported in detail[5] and compared[6,7] with a bench mark solution. The present paper describes the development and characteristics of the bench mark solution in greater detail than previously published. It is hoped that it will lead to further contributions to the search for efficient, high accuracy methods for problems of this type.

Attention is drawn to the fact that, as a result of the availability of time for further computations, the bench mark solution has been refined since Reference 6 was written, and the present results—which are the same as those in Reference 7—differ to a very slight extent from those previously published.

THE PROBLEM

The problem being considered is that of the two-dimensional flow of a Boussinesq fluid of Prandtl number 0·71 in an upright square cavity of side L. Both velocity components are zero on the boundaries. The horizontal walls are insulated, and the vertical sides are at temperatures T_h and T_c.

The solutions of this problem—velocities, temperature and rates of heat transfer—have been obtained at Rayleigh numbers of 10^3, 10^4, 10^5 and 10^6.

MATHEMATICAL FORMULATION AND METHOD OF SOLUTION

The stream function–vorticity (ψ–ζ) formulation of the problem was used. We choose the quantities L, κ (the thermal diffusivity) and L^2/κ as scale factors for length, stream function and time, and introduce $T = (T' - T_c)/(T_h - T_c)$, where T' is the local dimensional temperature. We use axes labelled (x, z), with z vertically upwards. The non-dimensional equations are then

$$\frac{\partial}{\partial x}(u\zeta) + \frac{\partial}{\partial z}(w\zeta) = \Pr \nabla^2 \zeta + \mathrm{Ra}\Pr \frac{\partial T}{\partial x}$$

$$0 = \nabla^2 \psi + \zeta$$

$$\frac{\partial}{\partial x}(uT) + \frac{\partial}{\partial z}(wT) = \nabla^2 T.$$

These equations were modified to allow the use of the method of the false transient[8] by the inclusion, on the left hand sides of each, of the terms

$$\frac{1}{\alpha_\zeta}\frac{\partial \zeta}{\partial t}, \quad \frac{1}{\alpha_\psi}\frac{\partial \psi}{\partial t}, \quad \text{and} \quad \frac{1}{\alpha_T}\frac{\partial T}{\partial t}$$

respectively. As $t \rightarrow \infty$ and a steady state is approached, the equations revert to their correct forms and the true steady solution (if one exists) is achieved. The coefficients α_ζ, α_ψ and α_T provide extra degrees of freedom to control stability and the rate of approach to the steady state.

The modified equations were solved on a square mesh by a finite difference method; forward differences were used for the time derivatives and second-order central differences for all space derivatives. The resulting finite difference approximations were solved by an alternating-direction implicit algorithm.

This method is not advanced as being particularly accurate in itself: it yields a standard second-order solution. But it is efficient; it allows solutions to be found at conditions under which the normal FTCS method is unstable; and the retention of a uniform mesh facilitates the application to the solutions of an extrapolation process. Richardson's extrapolation has been used; this leads to the high accuracy bench mark solution described here.

THE CALCULATION OF HEAT FLUX

From the viewpoint of an engineer, the most important characteristic of the flow is probably the rate of heat transfer across the cavity.

The local heat flux in a horizontal direction at any point in the cavity is

$$Q(x, z) = uT - \partial T/\partial x.$$

(On the boundaries, $u = 0$.) The quantity Q was calculated at all mesh points. Except at $x = 0$ and $x = 1$, $\partial T/\partial x$ was found using a second-order central difference approximation.

Previous numerical experiments[9–10] had suggested that, at the vertical boundaries, the first-order (two point) approximation to $\partial T/\partial x$ should be used. It had been found to lead to values of wall heat flux which were less sensitive to variations in mesh size than those obtained using a second-order formula and therefore, for any non-zero mesh size, more accurate. To test this suggestion further, the heat flux $Q(0, z)$ at the boundary was computed for each Rayleigh number and mesh size with formulae of the first to the fourth orders. The

average Nusselt number on the boundary, Nu_0, was then found by numerical integration using Simpson's rule.

Some of the initial results—those for $Ra = 10^3$ and 10^6—are shown in Figure 1. The values of Nu_0, as a function of the mesh size h, appear to be converging for each differentiation formula to the same value, as indicated by an arrow on the Nu axis. (The indicated value is the bench mark value, found as described below.) For each mesh size used, the second-order formula performs better than any of the others in almost every case. The results for $Ra = 10^4$ and 10^5 have similar characteristics and support this assertion. The solutions presented below were therefore obtained using a second-order approximation at the wall, as well as within the cavity.

The reason for the disagreement with the previous numerical experiments is not known. One of these[9] concerned convection inside a cylinder, for which the temperature field near the wall would be different from—and apparently more nearly linear than—that found here. In a study[10] of convection in a rectangular cavity, a first-order approximation was found to be better for a Boussinesq fluid, but a second-order approximation was better when fluid property variations were incorporated into the analysis. One would have expected that approximations of the same order should be used throughout the calculations. That was found to be the case here, but apparently is not always true. In particular, the present results
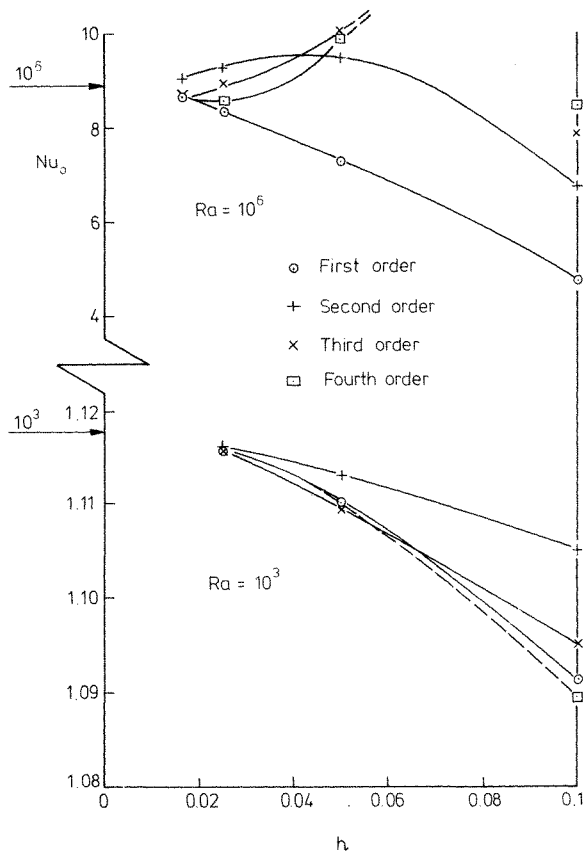

Figure 1. Nu_0 as a function of mesh size and differentiation
formula for $Ra = 10^3$ and 10^6

show that the thin thermal boundary layer associated with high Rayleigh numbers can be well represented by a high-order approximation. But in the absence of knowledge of the correct value, a second-order approximation is now regarded as the most appropriate and was used to obtain all the results presented here.

THE ORIGINAL SOLUTIONS

For Ra of 10^3 and 10^4, solutions were found using uniform meshes from 11×11 to 41×41; at the higher values of Ra, finer meshes up to 81×81 were also used.

One of the complications of numerical fluid dynamics is the amount of computer output generated. Since the purpose of the present work is to find accurate values for quantities which can be readily compared, only some salient features of the flow are given here: those requested in References 2–4 and a few others.

Tables I to IV show, for the four Rayleigh numbers, and for the various mesh sizes, the following quantities:

$|\psi|_{mid}$ the stream function at the mid-point of the cavity;

$|\psi|_{max}$ the maximum absolute value of the stream function (together with its location): for Ra = 10^5 and 10^6, the maximum does not occur at the cavity mid-point;
and 10^6, the maximum does not occur at the cavity mid-point;

u_{max} the maximum horizontal velocity on the vertical mid-plane of the cavity (together with its location);

w_{max} the maximum vertical velocity on the horizontal mid-plane of the cavity (together with its location);

$\overline{Nu}$ the average Nusselt number throughout the cavity;

$Nu_{1/2}$ the average Nusselt number on the vertical mid-plane of the cavity;

Nu_0 the average Nusselt number on the vertical boundary of the cavity at $x = 0$;

Nu_{max} the maximum value of the local Nusselt number on the boundary at $x = 0$ (together with its location);

Nu_{min} the minimum value of the local Nusselt number on the boundary at $x = 0$ (together with its location).

The values given in the tables here and below for maximum (and minimum) quantities are not necessarily the largest (and smallest) mesh point quantities. They, and their locations, were computed by numerical differentiation using a fourth-order polynomial approximation; the evaluation and location of the maximum stream function required double differentiation. The interpolated maximum (minimum) values differed from the closest of the adjacent mesh point values by no more than 1 per cent in every case except one; the interpolated value of w_{max} at Ra = 10^6 was 6 per cent greater than the largest of the adjacent mesh point values.

Table I. The original solutions at Ra = 10^3

Mesh size	$|\psi_{mid}|$	$|\psi|_{max}$ x, z	u_{max} z	w_{max} x	$\overline{Nu}$	$Nu_{\frac{1}{2}}$	Nu_0	Nu_{max} z	Nu_{min} z
0·1	1·181	— —	3·427 0·801	3·449 0·193	1·096	1·104	1·105	1·462 0·141	0·723 0·936
0·05	1·174	— —	3·589 0·811	3·629 0·181	1·111	1·114	1·113	1·491 0·112	0·702 1
0·025	1·174	— —	3·634 0·813	3·679 0·179	1·116	1·117	1·116	1·501 0·087	0·694 1

Table II. The original solutions at $Ra = 10^4$

Mesh size	$|\psi_{mid}|$	$|\psi|_{max}$ x, z	u_{max} z	w_{max} x	$\overline{Nu}$	$Nu_{\frac{1}{2}}$	Nu_0	Nu_{max} z	Nu_{min} z
0·1	5·529	— —	16·243 0·808	18·055 0·139	2·171	2·170	2·307	3·637 0·211	0·676 1
0·05	5·176	— —	16·189 0·820	19·197 0·125	2·212	2·213	2·255	3·603 0·165	0·610 1
0·025	5·098	— —	16·182 0·823	19·509 0·120	2·234	2·235	2·242	3·545 0·149	0·592 1

Table III. The original solutions at $Ra = 10^5$

Mesh size	$|\psi_{mid}|$	$|\psi|_{max}$ x, z	u_{max} z	w_{max} x	$\overline{Nu}$	$Nu_{\frac{1}{2}}$	Nu_0	Nu_{max} z	Nu_{min} z
0·1	11·97	12·68* 0·3*, 0·6*	40·90 0·846	59·71 0·083	4·446	4·381	4·767	6·538 0·218	1·516 1
0·05	9·702	10·236 0·291, 0·601	36·46 0·854	62·79 0·075	4·454	4·455	4·716	7·901 0·133	0·797 0·973
0·025	9·234	9·739 0·286, 0·602	35·07 0·855	66·73 0·068	4·487	4·491	4·564	7·905 0·095	0·755 1
0·016	9·164	9·667 0·285, 0·601	34·87 0·855	67·91 0·067	4·503	4·506	4·531	7·802 0·087	0·741 1
0·0125	9·142	9·644 0·285, 0·602	34·81 0·855	68·22 0·066	4·510	4·512	4·523	7·761 0·085	0·736 1

* Mesh point values (see text)

Table IV. The original solutions at $Ra = 10^6$

Mesh size	$|\psi_{mid}|$	$|\psi|_{max}$ x, z	u_{max} z	w_{max} x	$\overline{Nu}$	$Nu_{\frac{1}{2}}$	Nu_0	Nu_{max} z	Nu_{min} z
0·1	32·93	46·41* 0·5*, 0·7*	230·22 0·915	213·91 0·0670	6·105	5·296	6·790	7·959 0·138	3·853 1
0·05	20·16	20·914 0·149, 0·554	79·27 0·862	195·44 0·0447	9·027	9·214	9·502	14·215 0·124	1·749 1
0·025	17·15	17·613 0·151, 0·542	67·49 0·854	206·32 0·0423	8·811	8·869	9·270	17·947 0·0675	1·015 0·984
0·016	16·67	17·113 0·151, 0·541	65·81 0·852	214·64 0·0396	8·794	8·823	9·035	18·255 0·0523	1·020 1
0·0125	16·53	16·961 0·151, 0·543	65·33 0·851	216·75 0·0387	8·798	8·816	8·928	18·076 0·0456	1·005 1

* Mesh point values (see text)

Although the effect of interpolation was generally small as far as the values themselves were concerned, it enabled the location of the extreme values to be found more precisely. The values and locations which are given in the tables for ψ_{max} at Ra $= 10^5$ and 10^6 using $h = 0\cdot1$ are not interpolated values but the relevant mesh point values; the solution is so distorted that numerical differentiation cannot be conveniently performed.

These tables show the not unexpected result that the process used is convergent; that the coarse mesh, high Rayleigh number solutions are useless; and that in the absence of some other technique such as extrapolation, even finer meshes would be required to obtain mesh size independence to a target accuracy of, say, $0\cdot1$ per cent.

EXTRAPOLATED SOLUTIONS

With results for several mesh sizes available, an extrapolation scheme can be used to generate a solution of greater accuracy.

If the order of the truncation error of the solutions is not known, it can be estimated from the results for three different mesh sizes, provided of course they have a set of mesh points in common. Thus three 11×11 matrices can be extracted from the three original solutions at $h = 0\cdot1$, $h = 0\cdot05$ and $h = 0\cdot025$; and three 21×21 matrices can be extracted from solutions at $h = 0\cdot025$, $h = 0\cdot01\dot{6}$ and $h = 0\cdot0125$.

Suppose X_t is the true value at a mesh point of a quantity of which the value computed using a mesh size of h_i is X_i; then

$$X_t = X_i + Ch_i^n, \qquad i = 1, 2, 3$$

where n is the order of the truncation error and C is assumed to be independent of h. It follows that n is given by the solution of

$$\frac{X_1 - X_2}{X_2 - X_3} = \frac{h_1^n - h_2^n}{h_2^n - h_3^n}$$

at each mesh point; or if $h_1/h_2 = h_2/h_3 = \lambda$ say, then

$$n = \ln \frac{X_1 - X_2}{X_2 - X_3} \bigg/ \ln \lambda.$$

The 'constant' C can then be found at each mesh point and hence the true value X_t can be obtained.

Calculations of this nature were performed for various combinations of solutions. The coarse mesh, high Rayleigh number solutions are clearly unreliable and were excluded; but otherwise the extrapolation yielded results that were at least plausible.

It was found, however, that the value of n varied throughout the cavity: from around 1 or even a little less to about 3 or even a little more. The average value of n was generally, but not always, quite close to the expected value of 2. There are two related reasons for this. First, the necessity to use three mesh sizes to calculate n meant that one relatively coarse solution had to be included. This contaminated the extrapolated solution, sometimes quite badly. Secondly, the computed value of the quantity C is not truly constant until the limit $h \to 0$ is reached—which, of course, it never is.

An extrapolation was then performed using not the local value of n computed at each mesh point for each variable but the average of those values for each variable. As mentioned, these averages were not always close to 2 and it was therefore felt, in retrospect, that unless this condition had been achieved, the extrapolated values would not be reliable.

After much exploration of these and some other extrapolation procedures, it was decided that use had to be restricted to the solutions obtained using two fine mesh sizes at each Ra, namely $h = 0.05$ and $h = 0.025$ at $Ra \leqslant 10^4$ and $h = 0.025$ and $h = 0.0125$ at $Ra \geqslant 10^5$. This enabled 21×21 solutions to be constructed at the two lower Rayleigh numbers, and 41×41 solutions at the two higher values. The use of $h = 0.016$ at the higher Ra was not convenient because it would have restricted the mesh size of the extrapolated solution to 0.05.

In consequence of performing extrapolation using only two solutions, it had to be assumed that $n = 2$. The method used is second order, a rate of convergence which is progressively approached as the mesh size is reduced. In limiting attention to two fine mesh solutions it is implied that true quadratic convergence has in fact been reached.

This extrapolation procedure failed in one case: in the determination of Nu_{max} at $Ra = 10^6$, the value of which proved to be exceptionally sensitive to the method of its calculation. Figure 2 shows the variation of Nu along the lower part of the heated wall for the three finest grids used. At $z = 0$, Nu increases with decreasing grid size; at $z = 0.1$, Nu decreases; and Nu_{max}, which occurs in the interval $0 \leqslant z \leqslant 0.1$, is not monotonic. It turns out that extrapolation from the solutions found at $h = 0.025$ and 0.0125 yields a value for Nu_{max} which is greater than the 0.0125 value, whereas examination of the 0.016 and 0.0125 solutions, as illustrated in Figure 2, suggests that the zero mesh size value should be smaller.

For this one case, therefore, values of Nu at $x = 0$ and near $z = 0$ were extracted at intervals of 0.05 from the 0.016 and the 0.0125 solutions. This has the advantage that use is made of solutions found with the two finest meshes, and the disadvantage that these meshes have fewer points in common. Extrapolation was applied to these values, using $n = 2$, and numerical differentiation then used to locate the maximum.

THE BENCH MARK SOLUTION

Table V shows the results of the extrapolation process: the bench mark solution. Again, only selected quantities are presented here. Copies of the full output are available on request.
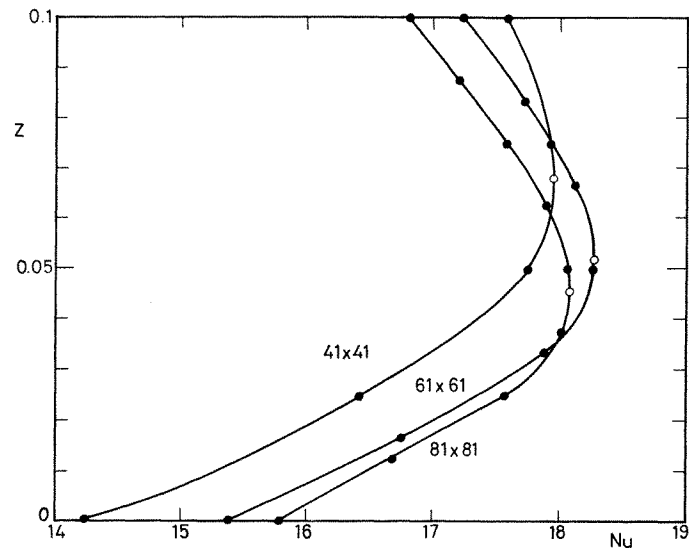

Figure 2. The variation of local Nusselt number along the lower part of
the heated wall computed for three different mesh sizes. $Ra = 10^6$
● Computed points; ○ Interpolated maxima

Table V. The bench mark solution

	Ra			
	10^3	10^4	10^5	
$|\psi_{mid}|$	1·174	5·071	9·111	16·32
$|\psi|_{max}$	—	—	9·612	16·750
x, z	—	—	0·285, 0·601	0·151, 0·547
u_{max}	3·649	16·178	34·73	64·63
z	0·813	0·823	0·855	0·850
w_{max}	3·697	19·617	68·59	219·36
x	0·178	0·119	0·066	0·0379
$\overline{Nu}$	1·118	2·243	4·519	8·800
$Nu_{\frac{1}{2}}$	1·118	2·243	4·519	8·799
Nu_0	1·117	2·238	4·509	8·817
Nu_{max}	1·505	3·528	7·717	17·925
z	0·092	0·143	0·081	0·0378
Nu_{min}	0·692	0·586	0·729	0·989
z	1	1	1	1

The modified extrapolation procedure used for Nu_{max} was introduced after References 6 and 11 (an early version of this paper which was distributed at the Venice conference) were written. Some of the values in Table V differ from those in Reference 6, and Nu_{max} at $Ra = 10^6$ differs also from the value in Reference 11. The extent of the differences is displayed in the Appendix.

Figures 3–7 show the streamlines, isotherms, isovels and vorticity contours for the bench mark solution.

It is emphasized that extrapolation has been applied to all variables: to the primary solution variables ψ, ζ and T; to the secondary variables, the velocities u and w; and to the derived quantity Q, the heat flux across the cavity. If the velocities and heat flux of the extrapolated solution had been computed by differentiation of the extrapolated stream function and temperature respectively, the truncation errors of the numerical differentiation formulae—which in theory had been eliminated by extrapolation—would have been reintroduced.

By using extrapolation on the secondary and derived variables, the complete bench mark solution set is no longer internally consistent: the values of all the variables do not satisfy a system of finite difference approximations. Velocity in the bench mark solution is not the result of numerical differentiation of the bench mark values of stream function; and the bench mark heat flux cannot be computed from the bench mark temperature and velocity. Instead, the values of the bench mark variables are, within the limits of accuracy of the extrapolation process, a 21×21 or 41×41 subset of the internally consistent solution which would be obtained if it were possible to perform the computations using a mesh size of zero.

DISCUSSION

An assessment of the validity of the assumption that $n = 2$ may be obtained by examining the behaviour of the error in the computed solutions, the error being taken as the difference between those solutions and the extrapolated (true?) solutions.
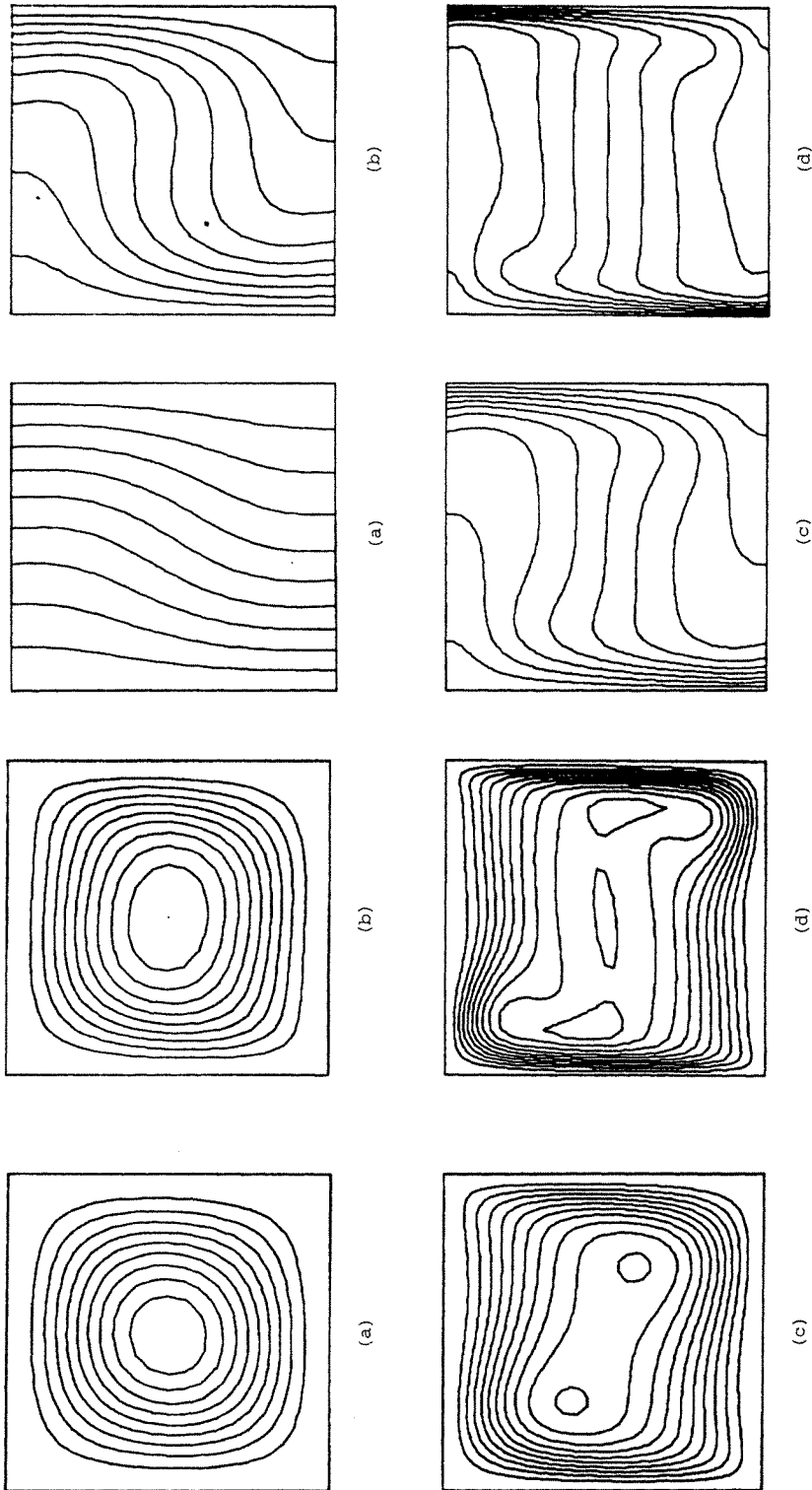
Figure 3. Contour maps of stream function ψ:
(a) Ra = 10^3; contours at $-1\cdot174(0\cdot1174)0$;
(b) Ra = 10^4; contours at $-5\cdot071(0\cdot5071)0$;
(c) Ra = 10^5; contours at $-9\cdot507$, $-8\cdot646(0\cdot9607)0$;
(d) Ra = 10^6; contours at $-16\cdot27$, $-15\cdot07(1\cdot675)0$

Figure 4. Contour maps of temperature T:
(a) Ra = 10^3; (b) Ra = 10^4,
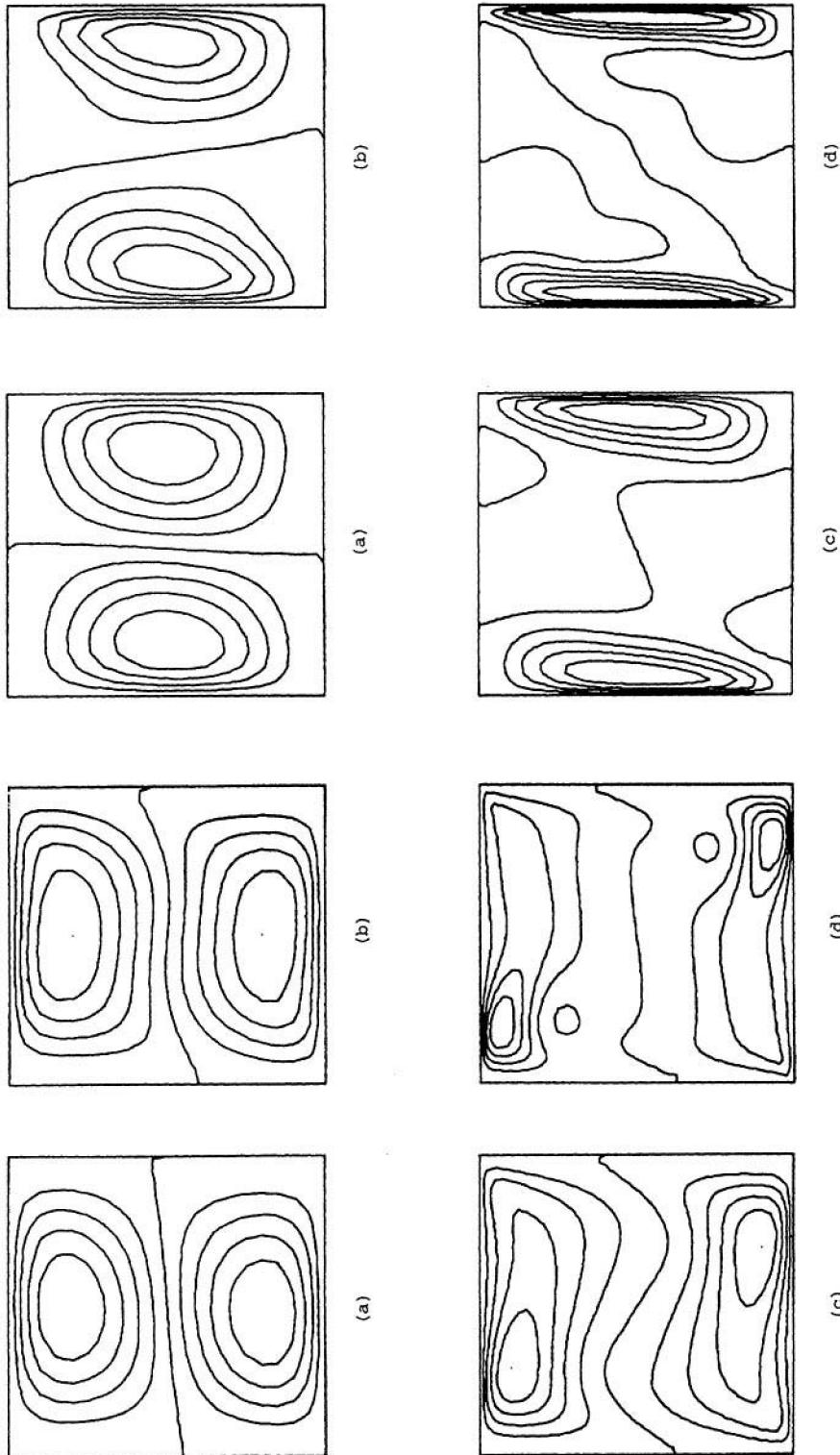(c) Ra = 10^5; (d) Ra = 10^6.
Contours at $0(0\cdot1)1$ in each case

Figure 5. Contour maps of horizontal velocity u:
(a) Ra = 10^3; contours at −3·637(0·7274)3·637;
(b) Ra = 10^4, contours at −16·00(3·200)16·00;
(c) Ra = 10^5; contours at −43·59(8·719)43·59;
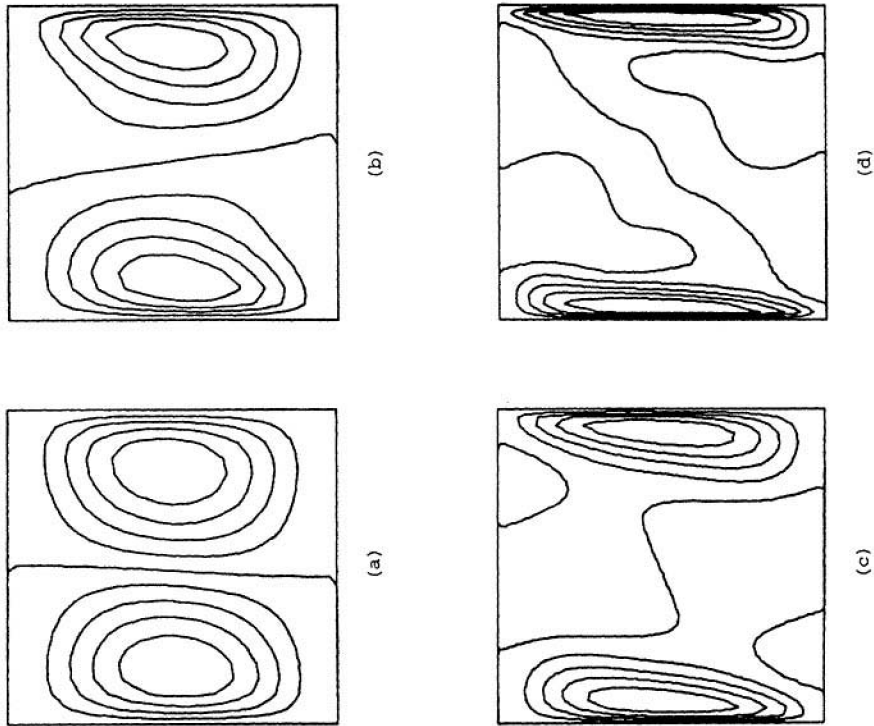(d) Ra = 10^6, contours at −125·5(25·10)125·5

Figure 6. Contour maps of vertical velocity w:
(a) Ra = 10^3; contours at −3·663(0·7327)3·663;
(b) Ra = 10^4, contours at −19·39(3·877)19·39;
(c) Ra = 10^5; contours at −67·96(13·59)67·96;
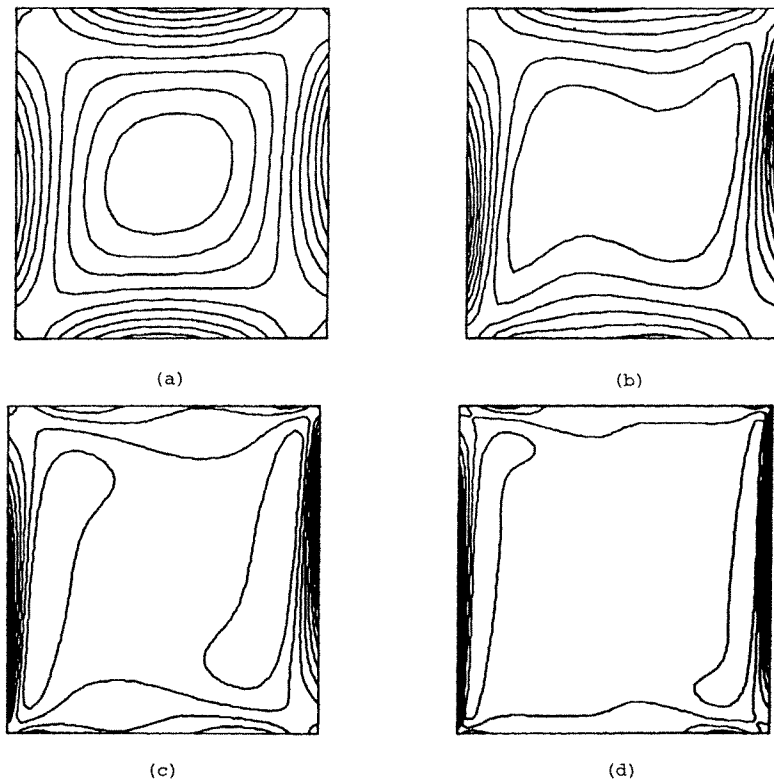(d) Ra = 10^6, contours at −207·6(41·52)207·6

(a)

(b)

(c)

(d)

Figure 7. Contour maps of vorticity ζ:
(a) $Ra = 10^3$; contours at $-32\cdot01(8\cdot328)51\cdot27$;
(b) $Ra = 10^4$; contours at $-124\cdot8(55\cdot17)426\cdot9$;
(c) $Ra = 10^5$; contours at $-600\cdot0(322\cdot6)2626$;
(d) $Ra = 10^6$; contours at $-3178(1847\cdot1)15293$

Table VI. Error (%) in some features of the original solutions

Ra	h	$|\psi_{mid}|$	w_{max}	$Nu_{\frac{1}{2}}$
10^3	0·1	0·6	−6·7	−1·3
	0·05	0·0	−1·8	−0·4
	0·025	0·0	−0·5	−0·1
10^4	0·1	9·0	−8·0	−3·3
	0·05	2·1	−2·1	−1·3
	0·025	0·6	−0·6	−0·4
10^5	0·1	31·4	−12·9	−3·1
	0·05	6·5	−8·5	−1·4
	0·025	1·4	−2·7	−0·6
	0·016̇	0·6	−1·0	−0·3
	0·0125	0·3	−0·5	−0·2
10^6	0·1	101·8	−2·5	−39·8
	0·05	23·5	−10·9	4·7
	0·025	5·1	−5·9	0·8
	0·016̇	2·2	−2·1	0·3
	0·0125	1·3	−1·2	0·2

Table VI shows these errors for three significant features of the flow: the mid-point stream function, the maximum vertical velocity on the horizontal mid-plane and the mid-plane Nusselt number. By and large, quadratic convergence is confirmed to an extent which is about as good as could be expected from such a complex numerical process. In particular, these and other results show that the rate of convergence is most nearly quadratic in ψ, ζ and T—the computed variables. With the derived quantities such as u, w and Nu the rate of convergence is generally somewhat less rapid. Figure 8 illustrates the rate of convergence for some characteristics of the solution other than those in Table VI: the mid-point vorticity and the temperature at the mid-point of the top of the cavity. The slopes of the lines, which have been drawn by eye, are all very close to 2 and again quadratic convergence is confirmed.

Figure 8 also provides at least qualitative support for believing the bench mark solutions to be accurate. For if the value adopted for X_t (i.e. the bench mark value) actually contained an error, then a log–log plot of $X_t - X_i$ against h would not produce a straight line.

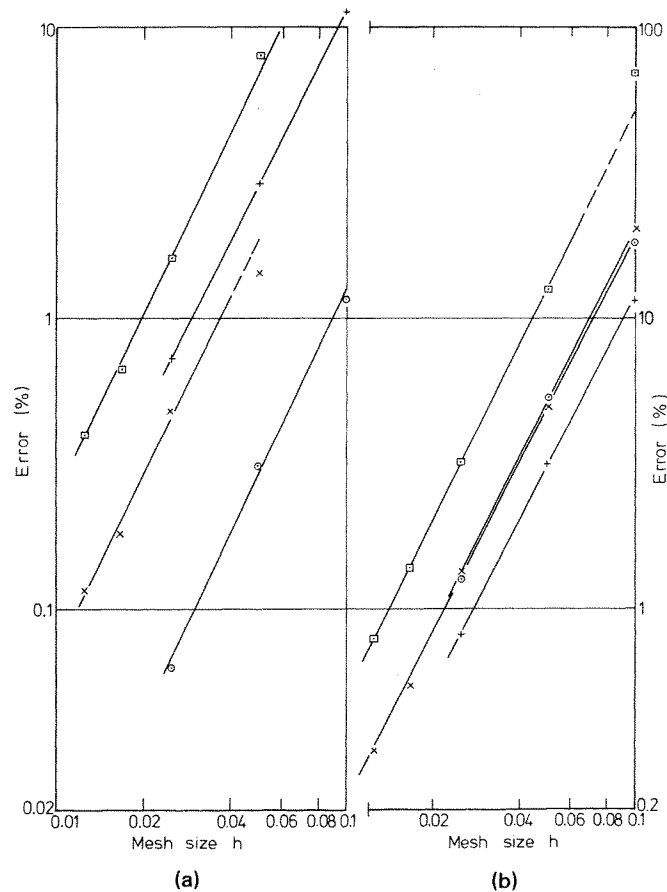Without knowing the correct solutions, of course, a quantitative assessment of the

Figure 8. Rates of convergence: (a) mid-point vorticity ζ_{mid};
(b) temperature at mid-point of top of cavity $T_{\frac{1}{2},1}$

$\odot$Ra $= 10^3$ $+$Ra $= 10^4 \times$Ra $= 10^5$ $\square$Ra $= 10^6$

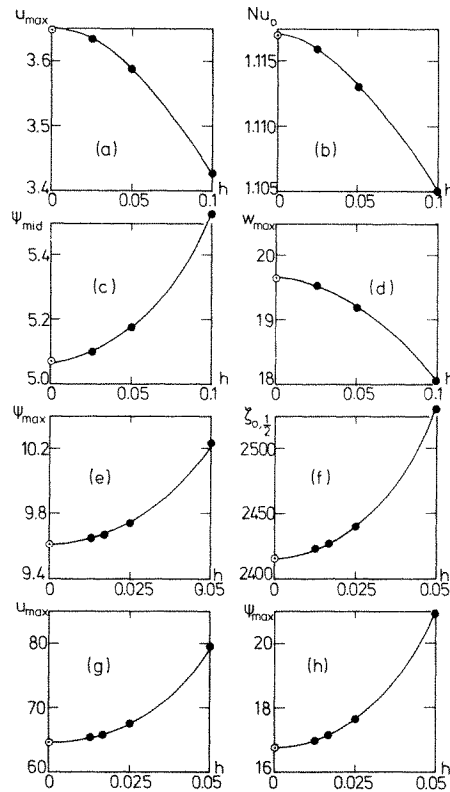(Note: Errors in ξ_{mid} at Ra $= 10^6$ are 10 times larger than values
shown in graph)

Figure 9. Convergence of the original solutions:
(a), (b): u_{max}, Nu_0 at $Ra = 10^3$;
(c), (d): $|\psi_{mid}|$, w_{max} at $Ra = 10^4$;
(e), (f): $|\psi|_{max}$, $\zeta_{0,\frac{1}{2}}$ at $Ra = 10^5$;
(g), (h): u_{max}, $|\psi|_{max}$ at $Ra = 10^6$

accuracy of the bench mark solutions is impossible to obtain. Figure 9 shows plots against h of several characteristics of the original solutions; the bench mark values are shown at $h = 0$. These and similar plots of other characteristics suggest the values shown in Table VII for the accuracy of the bench mark solutions. There will, of course, be some variation of accuracy among the various characteristics. However, these estimates are felt to be conservative and it is believed that the solutions presented here are therefore suitable for use as a bench mark against which other solutions can be compared.

Table VII. Estimated error of the bench mark solutions

Ra	Error (%)
10^3	0·1
10^4	0·2
10^5	0·3
10^6	1

WHICH NUSSELT NUMBER?

In a cavity with insulated horizontal boundaries, the heat flow across any line joining these boundaries—including the two vertical walls—must be the same. Through any line parallel to the z-axis, the heat flow is given by

$$\mathrm{Nu}_x = \int_0^1 Q(x, z)\, dz$$

and must be independent of x.

Figure 10 shows Nu_x—the integral having been calculated using Simpson's rule—as a function of x for the four extrapolated solutions. Also shown are the average values

$$\overline{\mathrm{Nu}} = \int_0^1 \mathrm{Nu}_x\, dx,$$

again found using Simpson's rule. Note that a very open scale has been used, which exaggerates the variation of Nu_x with x. The maximum relative difference between Nu_x and $\overline{\mathrm{Nu}}$ occurs, as would be expected, at the walls where the approximation used (although second order) is formally less accurate by a factor of two than a central difference
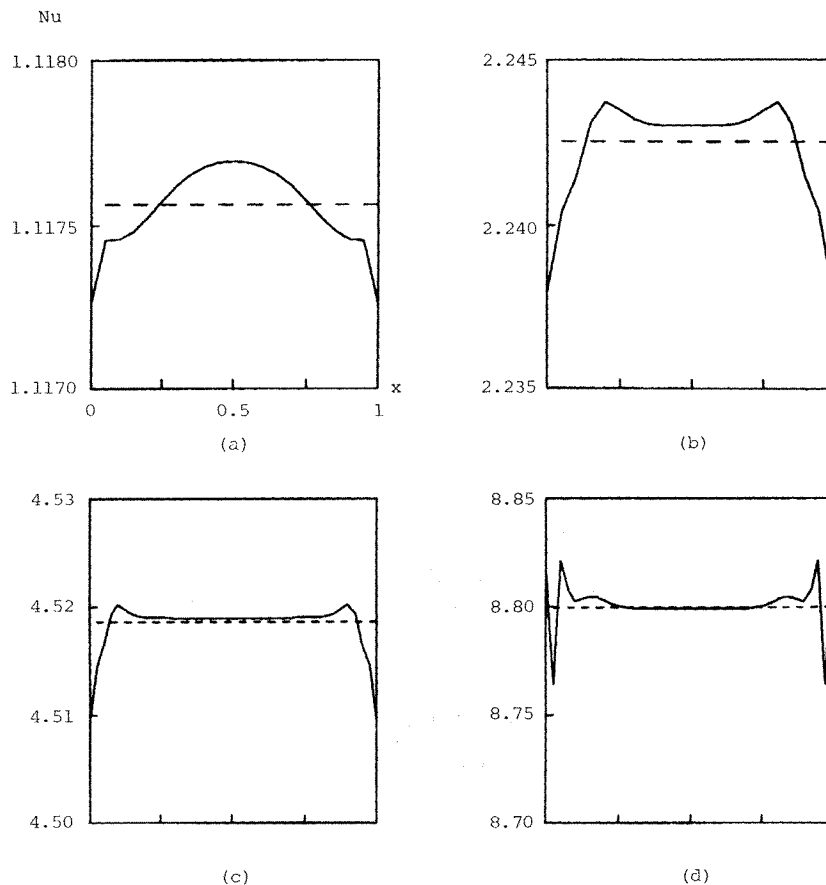

Figure 10. Nusselt number: (a) $\mathrm{Ra} = 10^3$, (b) $\mathrm{Ra} = 10^4$, (c) $\mathrm{Ra} = 10^5$, (d) $\mathrm{Ra} = 10^6$
———— Nu_x —————— $\overline{\mathrm{Nu}}$

approximation. These maximum differences are still very small: $0 \cdot 09$ per cent at $Ra = 10^3$, $0 \cdot 2$ per cent at 10^4 and 10^5 and $0 \cdot 4$ per cent at 10^6.

The mid-plane Nusselt number $Nu_{1/2}$ is sometimes given in papers. As Table V shows, this is a quantity which agrees extremely well with $\overline{Nu}$. The mid-plane value $Nu_{1/2}$ is easier to calculate than $\overline{Nu}$, and there is no reason to suppose that the latter is any more accurate. Indeed, it is probably less accurate, since it contains the wall values Nu_0 and Nu_1.

Accordingly, it is recommended that $Nu_{1/2}$ be adopted as the Nusselt number used to describe the heat flow across a cavity with adiabatic 'end' walls.

APPENDIX

Table VIII shows the differences between the bench mark solution and the solution presented in Reference 6. The latter was derived using a slightly different extrapolation process, and before the generation of the 81×81 solutions had been completed. Most of the differences are very small.

Table VIII. Differences (%) between bench mark solution and solution published in Reference 6

	Ra			
	10^3	10^4	10^5	10^6
$\|\psi_{mid}\|$	$0 \cdot 0$	$-0 \cdot 2$	$-0 \cdot 1$	$-0 \cdot 2$
$\|\psi\|_{max}$	—	—	$-0 \cdot 1$	$-0 \cdot 1$
u_{max}	$-0 \cdot 2$	$0 \cdot 0$	$-0 \cdot 1$	$-0 \cdot 5$
w_{max}	$-0 \cdot 1$	$-0 \cdot 1$	$0 \cdot 5$	$-0 \cdot 9$
$\overline{Nu}$	$0 \cdot 0$	$0 \cdot 2$	$0 \cdot 3$	$-1 \cdot 2$

REFERENCES

1. I. P. Jones, 'A comparison problem for numerical methods in fluid dynamics: the double-glazing problem', *Numerical Methods in Thermal Problems*, R. W. Lewis and K. Morgan (eds.), Pineridge Press, Swansea, U.K., 1979, pp. 338–348.
2. *Numerical Heat Transfer*, **2**, 395 (1979).
3. *J. Fluid Mech.*, **95**, 4, inside back cover (1979).
4. *Computers and Fluids*, **7**, 315 (1979).
5. I. P. Jones and C. P. Thomson (eds.), *Numerical Solutions for a Comparison Problem on Natural Convection in an Enclosed Cavity*, AERE–R9955, HMSO, 1981.
6. G. de Vahl Davis and I. P. Jones, 'Natural convection in a square cavity—a comparison exercise', *Numerical Methods in Thermal Problems*, vol. II, R. W. Lewis, K. Morgan and B. A. Schrefler (eds.), Pineridge Press, Swansea, U.K., 1981, pp. 552–572.
7. G. de Vahl Davis and I. P. Jones, 'Natural convection in a square cavity: a comparison exercise', *Int. j. numer. methods fluids*, **3**, 227–248 (1983).
8. G. D. Mallinson and G. de Vahl Davis, 'The method of the false transient for the solution of coupled partial differential equations', *J. Comp. Phys.*, **12**, 435 (1973).

9. S. S. Leong and G. de Vahl Davis, 'Natural convection in a horizontal cylinder', *Numerical Methods in Thermal Problems*, R. W. Lewis and K. Morgan (eds.), Pineridge Press, Swansea, U.K., 1979, pp. 287–296.
10. E. Leonardi and J. A. Reizes, 'Natural convection in a compressible fluid with variable properties', *Numerical Methods in Thermal Problems*, R. W. Lewis and K. Morgan (eds.), Pineridge Press, Swansea, U.K., 1979, pp. 297–306.
11. G. de Vahl Davis, 'Natural convection of air in a square cavity: an accurate numerical solution', Univ. of N.S.W. School of Mech. and Indust. Eng., *Report 1981/FMT/1* (1981).